Bioinspiration & Biomimetics

PAPER

Fin–fin interactions during locomotion in a simplified biomimetic fish model

RECEIVED
21 October 2020

REVISED
15 May 2021

ACCEPTED FOR PUBLICATION
20 May 2021

PUBLISHED
8 September 2021

David G Matthews[1,2,*] and George V Lauder[1,2]

[1] The Museum of Comparative Zoology, Harvard University, Cambridge, MA 02138, United States of America
[2] Department of Organismal and Evolutionary Biology, Harvard University, Cambridge, MA 02138, United States of America
[*] Author to whom any correspondence should be addressed.

E-mail: DaveMatthews@g.harvard.edu

Keywords: fish, robotics, leading edge vortex, fin–fin interaction

Supplementary material for this article is available online

Abstract

Fish median fins are extremely diverse, but their function is not yet fully understood. Various biological studies on fish and engineering studies on flapping foils have revealed that there are hydrodynamic interactions between fins arranged in tandem and that these interactions can lead to improved performance by the posterior fin. This performance improvement is often driven by the augmentation of a leading-edge vortex on the trailing fin. Past experimental studies have necessarily simplified fish anatomy to enable more detailed engineering analyses, but such simplifications then do not capture the complexities of an undulating fish-like body with fins attached. We present a flexible fish-like robotic model that better represents the kinematics of swimming fishes while still being simple enough to examine a range of morphologies and motion patterns. We then create statistical models that predict the individual effects of each kinematic and morphological variable. Our results demonstrate that having fins arranged in tandem on an undulating body can lead to more steady production of thrust forces determined by the distance between the fins and their relative motion. We find that these same variables also affect swimming speed. Specifically, when swimming at high frequencies, self-propelled speed decreases by 12%–26% due to out of phase fin motion. Flow visualization reveals that variation within this range is caused in part by fin–fin flow interactions that affect leading edge vortices. Our results indicate that undulatory swimmers should optimize both the positioning and relative motion of their median fins in order to reduce force oscillations and improve overall performance while swimming.

1. Introduction

Fishes have experienced a great deal of morphological evolution over their long evolutionary history, particularly in the number, position, and shape of their median fins [1]. This morphological evolution is often tied to ecological function [2–6], suggesting that this divergence can be adaptive. However, to fully understand the functional effects of variation in median fins we must first understand the individual role of each fin and how the fins might interact hydrodynamically. Although the caudal fin is often recognized as the major contributor to locomotor forces during steady swimming in many species [7–13], the dorsal and anal fins are also capable of actively flapping to produce thrust in body-caudal fin swimmers [7, 14–22]. However, the forces produced by the dorsal and anal fins tend to be lower than those generated by the tail [1, 13, 15, 23, 24]. In addition to generating thrust during steady swimming, the dorsal and anal fins aid in fast-start responses [25–27], turning [1, 10, 11, 15, 17, 18, 27, 28], and help stabilize the longitudinal axis of body against roll perturbations [17, 19, 27, 29, 30].

While the median fins may each function independently, their positioning along the body also allows them to interact hydrodynamically and alter each other's function. Many studies of live fishes have found that dorsal and anal fin wakes can interact with the caudal fin and suggest that this could alter the performance of the tail [1, 9, 10, 12, 13, 15–17, 19, 31, 32]. However, due to the limitations of working with live animals, few of these studies were able to test this hypothesis quantitatively. Instead, researchers have turned to mechanical systems and fluid simulations to understand fin–fin interactions and

we summarize a number of these recent studies in table 1.

Studies on simplified systems have largely been approached as engineering problems and have therefore not focused on replicating the hydrodynamics of fish (table 1). These studies tend to be carried out using either mechanical models or computational fluid dynamic (CFD) models of two independently actuated foils arranged in tandem. These models can cover a much broader parameter space than what a fish behaviorally exhibits, but as a result miss many of the higher-level details of a deforming fish body. For example, engineering models (table 1) lack a body joining the two independent fins, a feature which greatly affects the hydrodynamics of swimming fish [12, 13]. The fins on engineered foils also tend to be stiff, so the complex conformational changes seen in fish median fins are not replicated [18, 25, 26, 40]. Despite these differences, engineered models of fin–fin interactions have clearly shown that wake shed from one fin can increase both the efficiency and thrust production of a fin downstream and that this effect is highly sensitive to flapping frequency, fin spacing, and relative phase of the two fins (table 1). Furthermore, many of these studies show that augmentation of a leading-edge vortex (LEV) drives the change in performance [12, 13, 41, 42].

While studies of simple mechanical systems allow testing of a wide parameter space and energetics to be directly measured, CFD based on videos of live fish can provide further insights into the fluid dynamics of fin–fin interactions. This line of research has revealed that tuna finlets, carangid finlets, and bluegill dorsal/anal fins, for example, all create wakes that augment caudal fin performance [12, 13, 42, 43]. More specifically, these studies show that dorsal and anal fins typically produce more drag than thrust, but that the increase in caudal thrust due to interactions with the oncoming wake more than offsets this drag [12, 13, 42]. Similar to studies on two flapping foils, performance increases in CFD studies of fin–fin interactions are attributed to flow induced augmentation of LEVs [12, 13, 42]. While the complexity of these models allows us to gain deeper insights into fish hydrodynamics, it also reduces the size of the parameter space that can be explored, making it difficult to test a wide range of morphologies and behaviors.

In this study we aim to bridge the gap between robotic and biological experimental approaches by leveraging the experimental flexibility and energetic precision that robotic systems provide but doing so in an experimental system that more closely replicates the morphology and kinematics of fishes. We note that many of the past studies on fluid locomotion only make inferences about the effects of variables that they directly controlled. This has often led to either complex robotic models that are expensive and time consuming to build, or it has limited the scope of the results. We circumvent this tradeoff by

Table 1. Overview of a selection of past tandem foil studies. s is the spacing between foils, and C is the chord length of the foils.

Paper	Experimental/CFD	Phase differences	Foil spacing (s/C)	Stiffness	St	Re	Motion (pitch, heave)	Lateral forces reported	Force oscillation reported
Akhtar *et al* 2007 [33]	CFD	18–138°, by 15°	1	Stiff	0.19	600	Both	Only at 108°	No
Rival *et al* 2011 [34]	Both	0–120° by 30°	2	Carbon fiber, stiff	.08[a]	30 000	Both	No	No
Broering *et al* 2012 [35]	CFD	0, $\pi/2$, π	1	Stiff	0.3	10 000	Both	No	No
Boschitsch *et al* 2014 [36]	Experimental	0–2π, by $\pi/6$	.25–4.25, by .25	Aluminum, stiff	0.25	4700	Pitch only	No	No
Shoele and Zhu 2015 [37]	CFD	$-\pi$ to π	1.5, 2, 2.5	Flexible ray fins	0.4	400	Both	Yes	No
Muscutt *et al* 2017 [38]	CFD	0–2π	0.5–5, by 0.5	Stiff	0.2–0.5	7000	Both	No	No
Kurt and Moored 2018 [39]	Experimental	0–2π, by $\pi/12$	0.5–1.25 by .25	ABS, stiff	0.25	7500	Pitch only	Yes	No
This study	Experimental	21–115°[b]	1 or 2	Flexible	0.46–1.29[b]	27 000–106 000[b]	Both	Yes	Yes

[a]Not presented, calculated from data in paper.
[b]Indicates that the variable was not actively controlled but results from a passively controlled body.

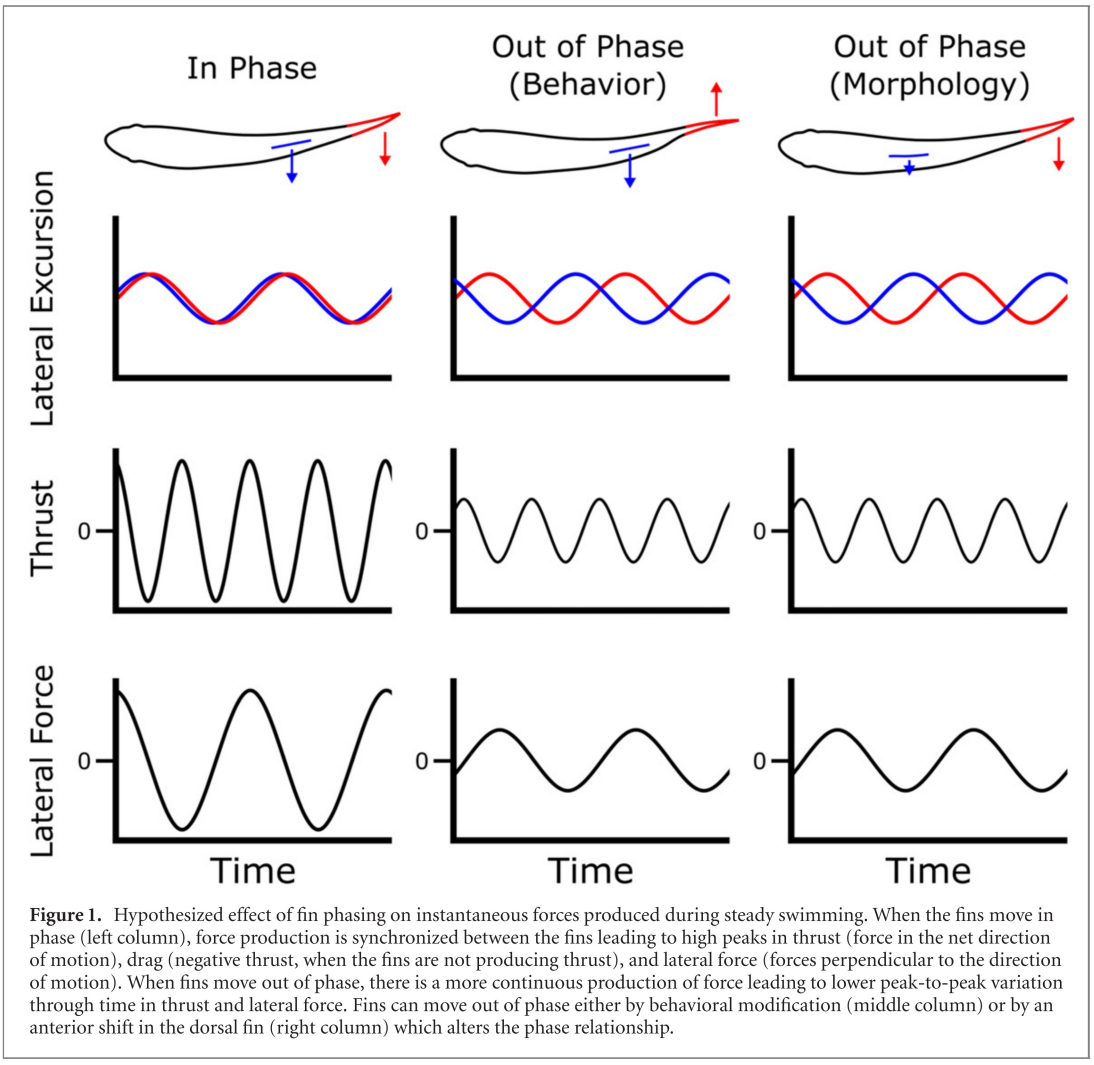

Figure 1. Hypothesized effect of fin phasing on instantaneous forces produced during steady swimming. When the fins move in phase (left column), force production is synchronized between the fins leading to high peaks in thrust (force in the net direction of motion), drag (negative thrust, when the fins are not producing thrust), and lateral force (forces perpendicular to the direction of motion). When fins move out of phase, there is a more continuous production of force leading to lower peak-to-peak variation through time in thrust and lateral force. Fins can move out of phase either by behavioral modification (middle column) or by an anterior shift in the dorsal fin (right column) which alters the phase relationship.

using a simple fish-like robotic system and measuring the emergent kinematics of the system instead of directly controlling them. By applying multivariate analysis to these measured traits, we are able to estimate their effects on swimming performance as if they had been controlled independently. We then employ flow visualization techniques to elucidate the physical mechanisms by which these variables affect swimming performance. Using this approach, we ask how fin position and relative timing of tandem median fins affect power consumption, propulsive economy, and the forces generated during swimming, examining both average forces as well as fluctuations in thrust and lateral forces over time.

Based on past studies we make two sets of predictions, the first regarding fin–fin flow interactions and the second relating to the unsteadiness of force production during undulatory swimming. First, we predict that flow from the dorsal and anal fin trailing edges will interact with the caudal fin and change the flow structure around this fin, altering the strength and stability of leading-edge vortices on the caudal fin. Specifically, we anticipate that the strength of the flow interactions will be primarily determined by the relative motion of the dorsal and anal fins with the caudal fin (phasing), but that the optimal phasing will change based on the inter-fin distance. In addition to altering flow interactions, several studies have suggested that out-of-phase fin motions will allow for more constant force production over the course of a flapping cycle [44–46]. Accordingly, our second prediction is that fins moving out of phase will cause a reduction in the oscillation of both thrust and lateral forces relative to in-phase force oscillation magnitudes (figure 1). The phase-lag between the fins is expected to be a direct result of body kinematics and fin position. This is the first experimental study that we are aware of to directly examine both the effects of fin–fin interactions and flapping synchronization between tandem fins on an undulatory body.

2. Materials and methods

We divide our variable space into three distinct types of variables. The first type are the control parameters. These are the variables that we directly control during

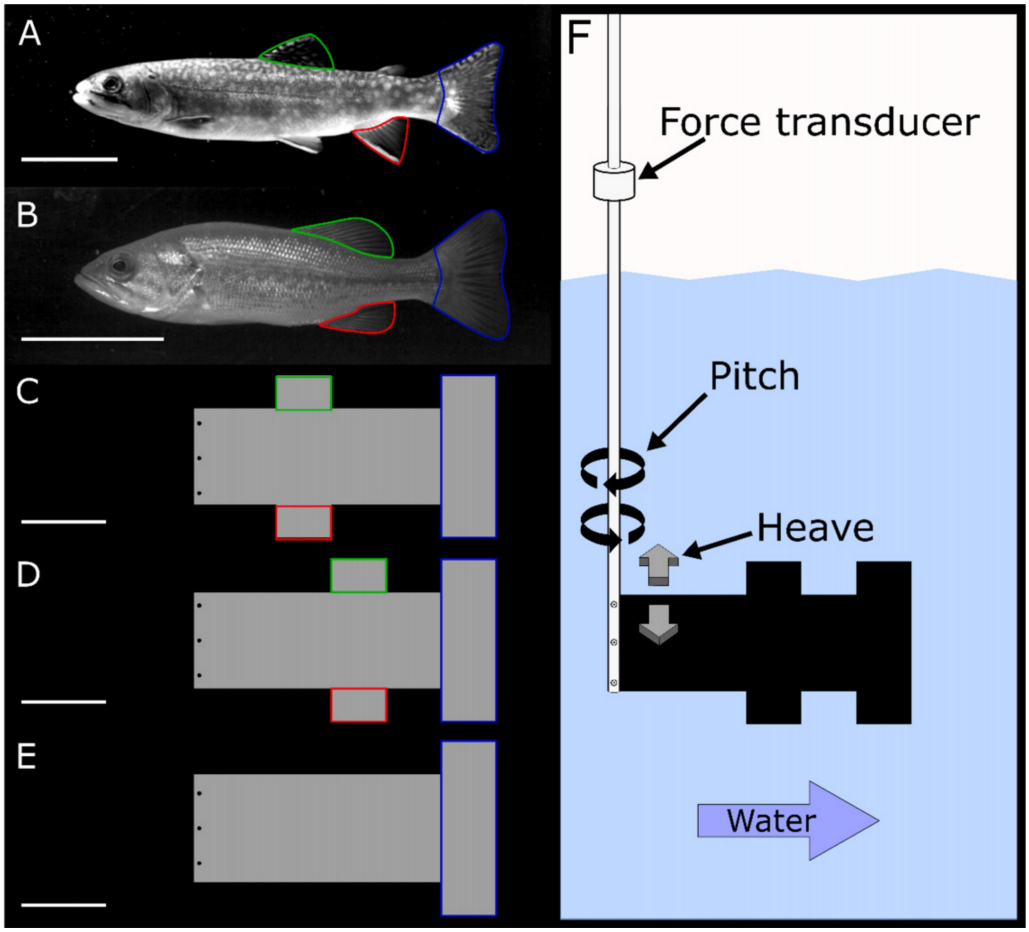

Figure 2. Plastic foils used in our experiments are based on body proportions and fin positions of real fish. (A) Brook trout (*Salvelinus fontinalis*). (B) Largemouth bass (*Micropterus salmoides*). (C)–(E) Experimental foils were cut from two different stiffness plastic sheets. Two of the foils have a dorsal fin and anal fin analogue, each one being 5% of the total surface area of the foil. (C) Foil with the dorsal and anal fins far from the caudal fin. (D) Foil with the dorsal and anal fins near the caudal fin. (E) The control foil has a wider central body structure so that the total surface area of the foil is the same as the foils withdorsal and anal fins. (A)–(E) Green and red outlines represent the dorsal and anal fins respectively, blue outlines represent the caudal fin. (F) Schematic of the foil in the recirculating flow tank demonstrating the two control parameters (pitch and heave) as well as the position of the force transducer. Scale bars on the left panels are 5 cm.

our experiments, and they include flapping frequency, fin spacing, and body stiffness. The next type is the emergent kinematics; the variables that are expected to affect swimming performance but are not directly controlled. These include the phase lag between the dorsal fin and the caudal fin as well as the peak-to-peak flapping amplitude of each fin. Finally, we measured and calculated various energetics variables so that we could characterize how well each model swam. These include the foil's self-propelled speed (SPS), power consumption, propulsive economy, and instantaneous oscillations in both thrust and lateral forces.

2.1. Foil design

To examine the effect of dorsal and anal fins on propulsion, we first designed three foils to mimic the lateral profiles of two ray-finned fish species that differ in their dorsal and anal fin placement (figures 2(C)–(E), supplemental figure 1(https://stacks.iop.org/BB/16/046023/mmedia)). These shapes correspond to a fish with anteriorly displaced fins (figure 2(C)), posteriorly displaced fins (figure 2(D)), or no dorsal and anal fin (control foil, figure 2(E)). These fin positions are not meant to exactly mimic any particular species, but rather are meant to capture some of the diversity seen across species. Specifically, we did not attempt to mimic asymmetrical fin positions (figure 2(A)) because this would reduce our ability to differentiate between the different fin positions. We measured the surface area of the dorsal and anal fins relative to the total lateral projected surface area of live fish (Brook trout *Salvelinus fontinalis*, Largemouth bass *Micropterus salmoides*, and yellow perch *Perca flavescens*) as they swam between one and two body lengths per second (supplemental table 1). We then designed our foils so the relative fin-size was similar to these fish, with the dorsal fin, anal fin, and each caudal fin lobe all having the same surface area. Although fin-size

was the same in all the foils, the body depth of the control foil was increased slightly to ensure that all three foils had the same total surface area. Finally, we used a laser cutter (Epilog Zing 24, Epilog Inc.) to cut each shape out of plastic shim stock (Artus Inc.). We used two different thicknesses of shim stock in order to examine the effect of material stiffness. Several of our previous projects have used this same set of materials to model flexible foil propulsion while varying stiffness [47–50]. The more flexible material was 0.4 mm thick and had flexural modulus $\sigma = 2.23$ GPa, while the stiff material was 0.75 mm thick with a flexural modulus $\sigma = 3.1$ GPa.

2.2. Experimental setup

2.2.1. Force data collection

We collected data using a robotic system suspended over a recirculating flow tank that is capable of moving both rigid and flexible foils in heave and pitch and controlling the phase and frequency of heave and pitch motions (figure 2(F)). This system has been used extensively [47, 48, 50–52] and detailed descriptions are provided in our previous publication [53]. The system drove the leading edge of each foil via a flat rigid rod suspended in the flow tank. Forces were measured using a six-axis force transducer (ATI Nano-17; ATI Inc., Apex, NC USA) attached to the rod. Trials were conducted by moving the leading edge of foils such that the lateral position (h) and pitch (α) followed $h = a\sin(2\pi ft)$ and $\alpha = \alpha_0 \sin(2\pi ft - \varphi)$, where a is the heave amplitude, f is the frequency, t is the time, α_0 is the maximum pitch angle, and φ is the phase lag between heave and pitch. During experiments we maintained a constant amplitude ($a = 2$ cm), maximum pitch angle ($\alpha_0 = 10^\circ$), with a phase lag ($\varphi = \pi/2$) between peak heave and peak pitch. Heave amplitude was chosen to be consistent with past studies using the same robotic system [47, 48] and pitch was chosen by testing several values and choosing the one that most resembled fish midline kinematics. While varying frequency in increments of 0.5 Hz (0.5–3.0 Hz in the flexible foil, 0.5–2.5 Hz in the stiff foil). Stiff foils were not flapped at 3.0 Hz because this generated forces above the load capacity of the force transducer. Our goal was to simulate the dynamics of foils swimming at a constant speed in an untethered environment, so we determined the flow tank speed at which the foil experienced zero net thrust (SPS). This was done by measuring the net thrust at five different flow speeds for each combination of foil shape, stiffness, and flapping frequency. We fit a linear regression of net thrust vs flow speed and then found the x-intercept of the regression line, giving the average speed at which net thrust equals zero (i.e. self-propulsion). We repeated this process 10 times for each frequency, stiffness, and shape combination, removed the highest and lowest SPS estimates, and averaged the rest of the values to get a final SPS estimate. We used this SPS estimate as the flow speed in the tank for all further trials at that parameter combination.

We then ran ten self-propelled trials at each flapping frequency and stiffness for all foil shapes. During each trial we measured positive and negative thrust forces (parallel to the net swimming direction) for 10 s at a frequency of 1000 Hz. Forces were recorded in the frame of reference of the pitching force transducer, and therefore did not always correspond to the net direction of motion. Raw data were trigonometrically corrected for the angle of the transducer to measure forces in the flow tank's frame of reference. Finally, data were smoothed with a lowpass Chebyshev filter (ripple = .5) using the R package signal (v0.7-6). Filter frequencies were chosen manually for each stiffness and frequency combination to be the lowest filter frequency that did not substantially decrease signal amplitude. The filter frequency was held constant across the different foil shapes. A custom R script (R v3.5.3, RStudio v1.0.153) was used to find all local extrema and then each local minimum was subtracted from the preceding local maximum to get the peak-to-peak displacement (referred to as ΔF_x and ΔF_y; figure 3). During data analysis, each pair of extrema was treated as an independent data point. In addition, we calculated average power consumption over the duration of each trial as

$$\overline{P} = \frac{\int_0^t \left(\frac{dY_{\text{pos}}}{dt} F_y + \frac{d\alpha}{dt} T_z\right) dt}{\Delta t},$$

where t is time, Y_{pos} is the heave position of the leading edge of the foil, F_y is the lateral force, α is the pitch angle, and T_z is the torque experienced as a result of pitching motion. Finally, we calculated propulsive economy as

$$\Omega = U_{\text{sps}}/\overline{P},$$

where U_{sps} is the self-propelled speed [49]. Propulsive economy is used instead of propulsive efficiency because our experiments are run at SPSs ($\overline{F_x} = 0$), and therefore propulsive efficiency is 0 [49].

2.2.2. Kinematics

During each set of self-propelled trials, we recorded one high speed video sequence from a ventral (bottom) view (at 125 Hz using a Photron UX100 high-speed camera; 1280 × 1024 pixel resolution, Photron, Inc.). From each video we digitized foil midlines from 10–12 frames evenly spaced over one complete flapping cycle using a custom MATLAB program (Mathworks Inc.). We also tracked the trailing edge of both the anal fin and the caudal fin on the foils to measure their flapping amplitudes and the phase shift between them.

In order to put the phase shift values in context we used previously-obtained videos from our research group of different fish species swimming steadily, and measured the phasing of their dorsal, anal, and caudal fins (bonnethead shark *Sphyrna tiburo*, chain dogfish shark *Scyliorhinus retifer*, yellowfin tuna *Thunnus*

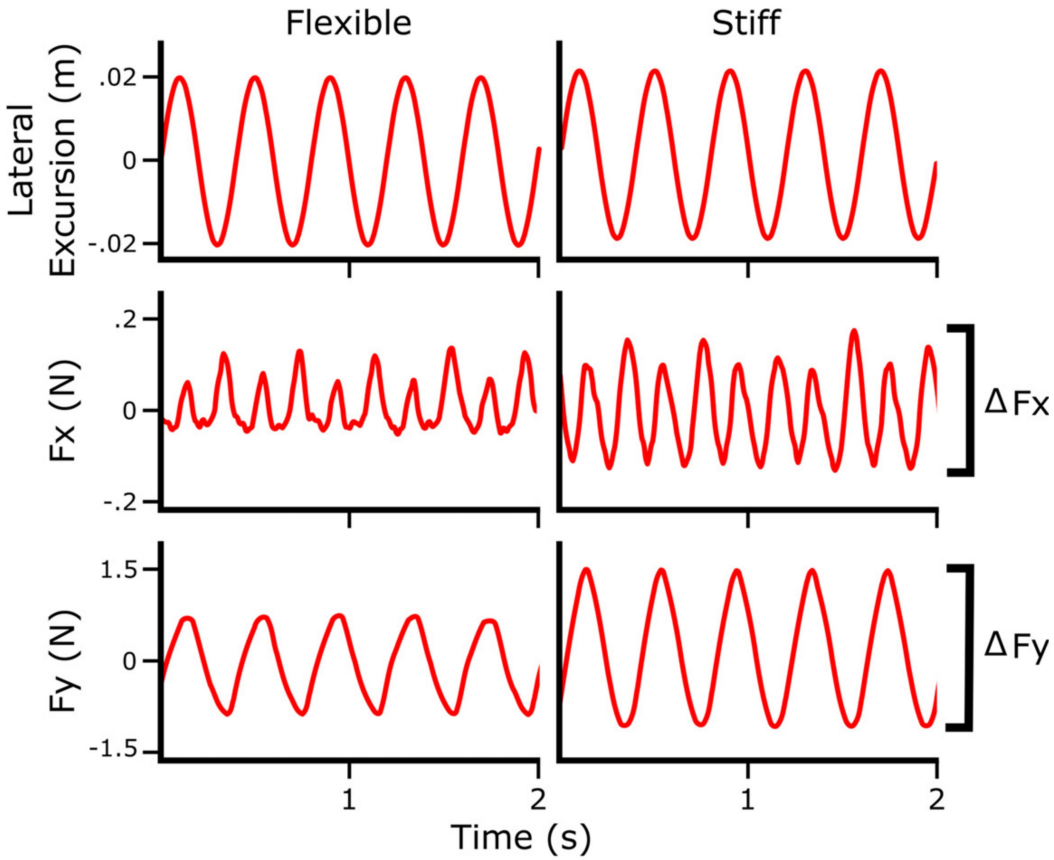

Figure 3. Low-pass filtered thrust and lateral forces fluctuate over the course of each flapping cycle. The difference between the peak and trough of forces in a flapping cycle (ΔF_x and ΔF_y) was used to represent steadiness of force production. These representative data are taken from trials run at 2.5 Hz using foils with the 'far' fin configuration (figure 2(C)).

albacares, largemouth bass *Micropterus salmoides*, yellow perch *Perca flavescens*, and brook trout *Salvelinus fontinalis*). We digitized the trailing edge of the caudal fin and either the dorsal or the anal fin depending on whether the videos showed a dorsal or ventral view. We characterised each species as having near fins, where the base of the digitized fin was directly adjacent to the caudal fin, or as having far fins. Since the dorsal and anal fins of trout are in different locations along the body, we digitized both and counted the dorsal fin as being far and the anal fin as being near to the caudal fin.

2.2.3. Particle image velocimetry (PIV)

We moved each foil at its maximum flapping frequency (3.0 Hz for flexible foils, 2.5 Hz for stiff foils) and with the flow speed set to the SPS. Maximum flapping frequencies were chosen for this experiment to maximize differences in flow around fins and in the resultant forces that they generate. We recorded water flow around the foil ventrally by illuminating nearly neutral plastic particles with two 5 W laser sheets (Optoengine, Midvale, Utah) placed on either side of the foil to prevent shadows. We placed the laser sheet horizontally such that it bisected both the anal fin and the ventral lobe of the caudal fin. All videos were recorded at 1000 Hz (Photron UX100 high-speed camera; 1280 × 1024 pixel resolution, Photron, Inc.), and the videos were analyzed in DaVis software (LaVision, Inc.) to obtain velocity fields (v7.2, 2pass 32 × 32 pixel area interrogation area). We subtracted average free-stream flow speed from each local flow velocity vector and visualized the vorticity of the resulting flow field. We examined flow at two time points that we predicted would be important for thrust generation. We first examined flow at the moment that the caudal fin begins lateral motion after reaching an amplitude maximum. This is when we observed the formation of a LEV and the fin is therefore susceptible to potential flow interactions. We also examined flow as the caudal fin was half-way through a flapping cycle to see if the LEV persisted.

In addition, to compare foil results with caudal fin surface flow patterns on live fish, experiments on freely-swimming bluegill sunfish (*Lepomis macrochirus*) were conducted to visualize flow leaving the dorsal fin and then interacting with the surface of the caudal fin. This species was chosen because they are commonly used as a model of teleost swimming hydrodynamics [1, 7, 10, 11, 13, 15, 18, 24]. Bluegill sunfish (4 fish, mean total length = 21 cm) swam in a recirculating flow tank at 1.1 L s^{-1}. A laser

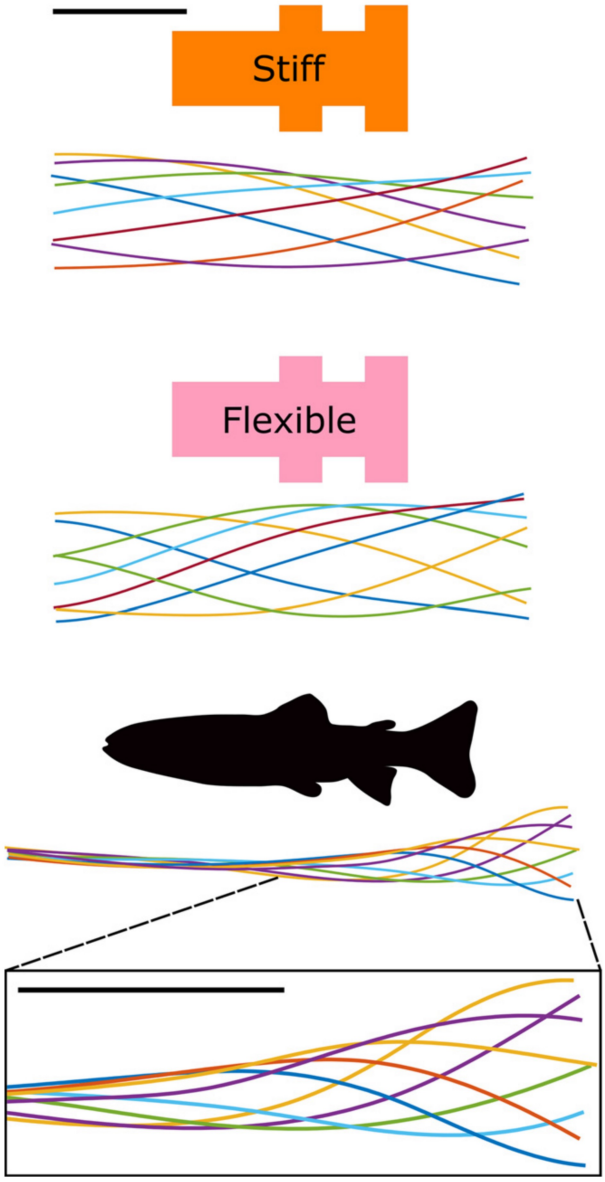

Figure 4. Midline traces throughout one flapping cycle are similar between the posterior half of a brook trout (*salvelinus fontinalis*) swimming at 1 L s^{-1} and foils swimming at 2.0 Hz, although foils show reduced growth in amplitude down the body relative to live fish. Specifically, the radius of curvature and general shape are similar between many individual time points in the foils and the trout. Different colors represent the midline at a different time in the flapping cycle. Scale bars are 5 cm.

light sheet was placed such that it intercepted the trailing edge of the dorsal fin, the gap between the dorsal and caudal fins, and the surface of the caudal fin. A Photron PCI-1024 high-speed camera captured video (500 fps) through a dorsal view mirror. Surface wave distortion was minimized by means of a floating transparent boat on the water surface.

2.3. Statistical analysis

Since flapping frequency is one of the primary control parameters that fish use to alter swimming behavior and performance [20, 54, 55] we used linear models to understand how force oscillation (ΔF_x and ΔF_y), SPS, power, and propulsive economy are each affected by flapping frequency in our model. Each of these energetics metrics was regressed independently against flapping frequency with fin position and body stiffness as categorical covariates. Since the model estimates the effect of categorical variables through changes to the y-intercept we did not fix this value at zero. Each regression was checked for heteroskedasticity and normality of the residuals to evaluate whether a linear fit of the data was appropriate. Models explaining each energetics metric besides SPS were heteroskedastic, so frequency was converted to an orthogonal quadratic and the regressions were run again. After this correction, all models had improved R^2 values, low heteroskedasticity, and normally distributed residuals. We then examined the coefficient estimates for each fin position and for the different

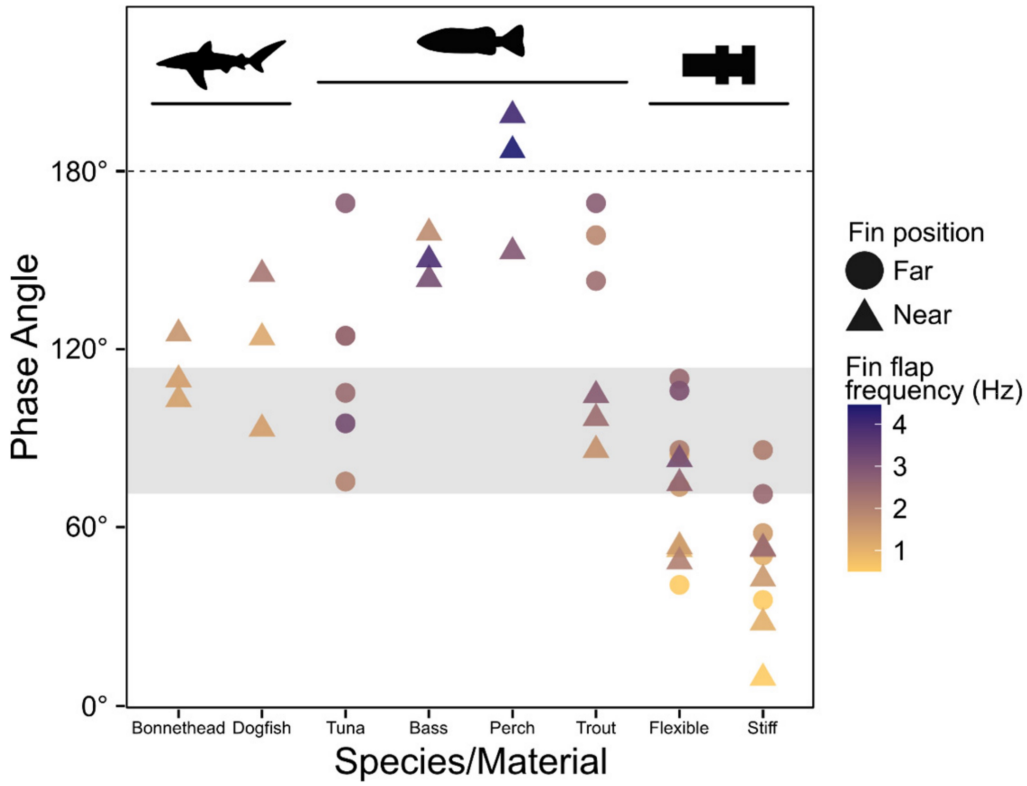

Figure 5. Fish and our flexible model each display a wide range of dorsal-caudal fin phasing, with some overlap between the two groups (shown as a gray band). A phase angle of 0° represents fins that are in phase and 180° represents fins that are out of phase. Fish data are recorded from the anal or dorsal fin, and are representative of both chondricthyans (sharks) and actinopterygians (ray-finned fishes). In order from left to right, the included species are the bonnethead shark (*Sphyrna tiburo*), chain dogfish shark (*Scyliorhinus retifer*), yellowfin tuna (*Thunnus albacares*), largemouth bass (*Micropterus salmoides*), yellow perch (*Perca flavescens*), and brook trout (*Salvelinus fontinalis*). In order from left to right, the two foil conditions are flexible and stiff, and are the same models as those used in all other experiments. Each point represents one trial. The number of individuals of each species ranges from 1–5 and fish are recorded swimming between 1–2 body lengths per second.

body stiffnesses to determine whether either variable could explain broad differences between the models. These estimates were converted to centered and standardized units for ease of comparison by subtracting the mean and dividing by the standard deviation separately in each continuous independent variable.

Although these initial models explain a majority of the variance in our energetics metrics, there is still variation between the different models that remains unexplained. To understand this residual variation, we added kinematic variables describing the exact motion of the fins to our existing multivariate models, maintaining the non-linearity of frequency when appropriate. Specifically, we added the peak-to-peak amplitude of the anal fin, peak-to-peak amplitude of the caudal fin, and the relative phasing of the two fins. Phase angle is known to have a sinusoidal effect on swimming performance in cases of fin–fin interactions, with a sin wavelength of approximately 360° [33]. Since the phase angles in our model had a maximum range of 22°–115°, we transformed phase angle to an orthogonal quadratic to approximate a small portion of the sin wave. Data from the control foil was excluded from this analysis because the phasing and anal fin amplitude were undefined in this model.

When constructing these models, we include an interaction between fin position and phase angle in addition to each variable's independent effect. This interaction is included to help us address the core question of how the relative motion of the fins affects swimming performance. Since we expect any such effect to come from altered flow environments, we cannot consider either fin motion parameter to act independently of the other. Accordingly, the interaction effect allows us to separately measure the effects of fin phasing on performance in the context of the near-fin foil and the far-fin foil.

To avoid overfitting the data, we next used a stepwise AICc process (Aikaike information criterion corrected for small sample size, presented in [56]) to choose the smallest set of explanatory variables that sufficiently predict a given energetics metric (SPS, ΔF_x, ΔF_y, power, or propulsive economy) [57]. This method works by comparing the base model to each possible model with one of the explanatory variables removed. It assigns an AICc score to each model by rewarding high explanatory power while penalizing

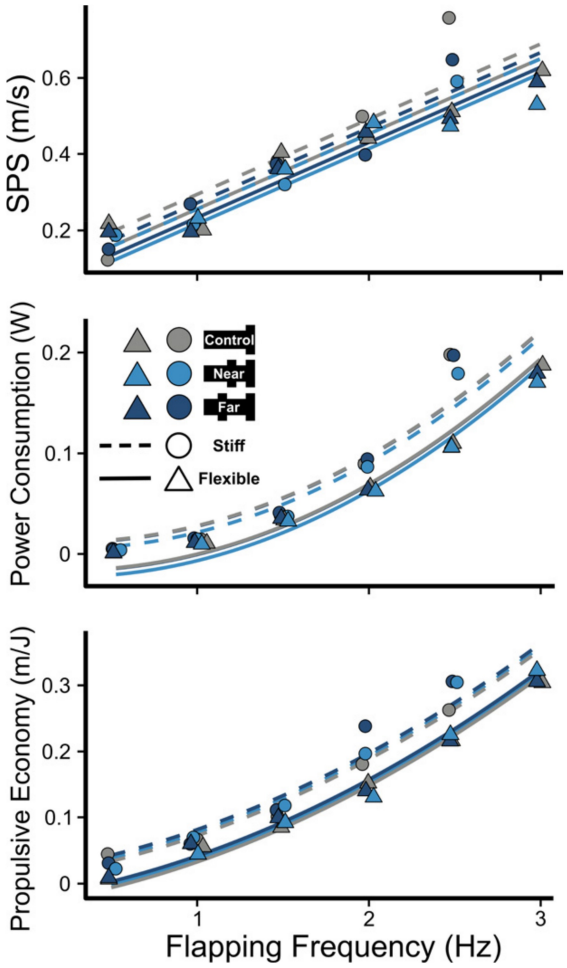

Figure 6. The relationship between flapping frequency and self-propelled swimming speed (SPS), power, and propulsive economy is significantly different between stiff and flexible foils. Without accounting for fin kinematics, fin position does not have a significant effect on this relationship. Complete linear regression coefficients and *p*-values are presented in supplemental table 2. Data were not collected at 0.5 Hz in the flexible near-fin foil. Horizontal jitter was has added to the data points to make overlapping values apparent.

for each variable. It then takes the best model (lowest AICc score) and repeats the process using this model as the new base model. This effectively removes all variables which individually add little explanatory power to the model. Once the analysis reaches a point where removing variables fails to improve the AICc score, we conclude that we have found the best model. The resultant models were then run to obtain final parameter estimates and were visually checked for heteroskedasticity and normality of residuals. These estimates were converted to centered and standardized units in the same manner as prior models. AICc was chosen instead of AIC for model selection to prevent overfitting because of our small sample size [57].

Finally, we used the model to produce estimates of the maximum SPS that would have been achieved in each combination of body shape and body stiffness if the fin phasing had been held at the optimal value within the range observed in that model. This was accomplished by finding the maximum SPS observed across all trials in each foil, then recording the maximum model output when the same parameter values are used with all possible phase angles seen in that particular model. We then divided the true maximum SPS by the predicted maximum SPS and subtracted that value from one to find the percent change in swim speed attributable to fin phasing. All analyses were run in R (v3.5.3).

3. Results

3.1. Comparison to live fish

Our foils were actuated at the leading edge with a pitching and heaving motion. This led to undulations passing down the length of the foil during locomotion and to the production of thrust. When compared to the swimming midline of a brook trout swimming at 1 body length per second (L s^{-1}), the primary difference was in the amount of anterior motion. This fish was chosen because it has often been used as a representative model of steady undulatory swimming

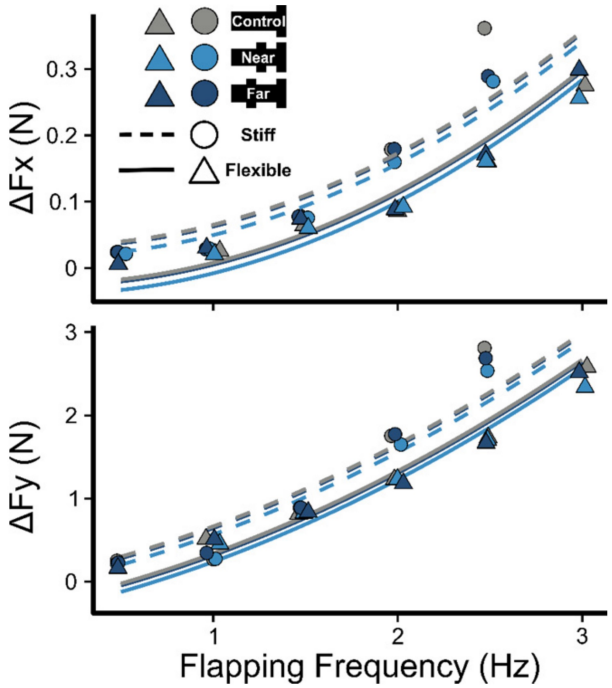

Figure 7. The relationship between flapping frequency and the amplitude of thrust (ΔF_x) and lateral force (ΔF_y) oscillation throughout a flapping cycle is significantly different between stiff and flexible foils. Without accounting for fin kinematics, fin position does not have a significant effect on this relationship. Complete linear regression coefficients and p-values are presented in supplemental table 2. Data were not collected at 0.5 Hz in the flexible near-fin foil. Horizontal jitter was has added to the data points to make overlapping values apparent.

[17, 19, 58]. The head of the trout undergoes low amplitude oscillations as it swims while our foils were programmed to heave at the leading edge (figure 4) and therefore had a similar undulation amplitude throughout the body. However, if we only consider the posterior (primarily propulsive) region of trout, the portion of the body containing the median fins, the midline trace is qualitatively similar to both of our foils. Specifically, we see similar radii of curvature and midline shapes in the experimental foils and in the trout.

Conversely, the relative phasing of the fins on the foils was largely dissimilar to the values seen in real fish (figure 5). Nevertheless, we believe that the comparison is informative since the total range of phasing values observed is similar between fish and our model. Across several species of both cartilaginous and bony fishes, the phasing of the trailing edge of the dorsal or anal fin with the trailing edge of the caudal fin ranged from 93°–197° when there was a gap between the fins and 83°–170° when the fins were directly adjacent. This variation likely comes from differences among the species in fin position, body flexibility, and behavior, particularly in species that can actively move their dorsal fin. The fin phasing of foils ranged from 22°–90° in foils with close fins and from 46°–115° in foils with distantly-spaced fins. Although there is overlap between the two ranges, the fins on our foils were generally more in phase than those in live fish. Our inability to replicate highly out of phase motions is likely explained by the limitations of a passively actuated body and the lack of active muscular control of the fins.

3.2. Forces and energetics

Since we ran all final trials at SPS the net thrust force is necessarily 0 (figure 3), and therefore is not reported. Instead, we present the SPS values as a proxy for the thrust force being generated. In the first set of models, those that only use control parameters as predictors, we found that all energetic variables significantly increased with frequency (table S2). Furthermore, all these metrics except SPS were best modeled as having a quadratic relationship with frequency (figures 6 and 7, table S2). The best model fit for SPS assumed a linear relationship with frequency (figure 6, table S2). We also found that stiffness was positively correlated with each energetic metric, although the effect on SPS was marginally significant ($p = .081$) and this effect was lost in later models (tables 2 and S4). In contrast, the shape of the foil did not have a significant effect on any of the energetics metrics (table S2).

It is not surprising that fin position was not broadly correlated with swimming performance given that the effect of fin position is complex and unlikely to be uniform across all frequencies and stiffnesses. To parse the true effect of the fin position we added fin kinematics to our models and conducted AICc analyses to select the smallest set of explanatory variables that could sufficiently predict each energetics

Table 2. Coefficient estimates for AIC selected models. All estimates are presented in standardized units and are therefore represent the change in the dependent variable associated with a one standard deviation increase in the corresponding independent variable. Positive and negative coefficients are represented with blue and red cells, respectively.

Dependant variable	Intercept	Frequency	Frequency^2	Stiffness (flexible → stiff)	Dorsal amplitude	Caudal amplitude	Position (near → far)	Phase angle	Phase angle^2	Position (n → f)	
										*Phase	*Phase^2
SPS (m s^{-1}) ($R^2 = .991$)	0.341	0.196	—	—	0.0293	−0.0198	0.0778	−0.129	−0.0343	0.0576	0.0312
Power consumption (W) ($R^2 = .990$)	0.0232	0.057	0.0359	0.0457	0.0149	−0.0104	—	−0.0288	−0.0283	0.0475	0.0113
Propulsive economy (m J^{-1}) ($R^2 = .990$)	0.0992	0.0716	0.0294	0.0976	0.0201	−0.0191	−0.037	0.0397	−0.00836	—	—
ΔF_x (N) ($R^2 = .995$)	0.0411	0.068	0.0569	0.101	0.0288	−0.0223	−0.0299	−0.0247	−0.0465	0.0723	0.0284
ΔF_y (N) ($R^2 = .998$)	0.638	0.588	0.365	0.817	0.293	−0.227	−0.321	−0.127[a]	−0.364	0.486	0.242

[a]Indicates a variable with $0.05 < p < 0.1$ that was kept by the model and is considered marginally significant.

metric (table S3). Each final model gives an estimate of the effect that each predictor variable has on the dependent variable after accounting for the effect of the other predictor variables. Importantly, this means that coefficient estimates of different predictors are independent of each other and can be interpreted individually. We present these coefficient estimates in standardized units for ease of comparison (table 2). Standardized coefficients should be interpreted as an estimated change in the dependent variable for one standard deviation change in a continuous independent variable. Quadratic coefficients should be interpreted by examining the sign of the linear term and the quadratic term. If the linear term is positive, then it implies a positive correlation with the response variable. Conversely, a negative linear term indicated a negative correlation with the response variable. A positive quadratic term implies that the effect is concave up. Paired with a positive linear term, this means that the rate of change of the response variable is positive (positive, concave up). A negative linear term with a positive quadratic means that the rate of change of the response is decreasing (negative concave up). The inverse is true for negative quadratic terms, leading to either a positive concave down (positive linear term) or a negative concave down (negative linear term) response. These patterns would not necessarily hold true if we wanted to estimate effects far from the mean, but since we centered our variables, they are generally correct. Finally, the interaction effect should be interpreted only when considering the far-fin foils. In the near fin foils, the effect of fin phasing on each energetics metric is given by the variables 'phase angle and phase angle^2'. To find the same predicted effect in the far-fin foils it is necessary to add the respective interaction effect terms to each of these independent variables.

A complete list of model coefficients can be found in tables 2 and S4, but for brevity we highlight some broader trends in the results. We only present the coefficient estimates from the statistical models with both controlled and kinematic variables because these have the most explanatory power. Any differences from earlier models of swimming energetics are due to unexplained variance in those models. It is also important to remember that positive changes in energetics variables are not always beneficial to performance, for example an increase in power consumption while maintaining the same swimming speed would not generally be considered beneficial. First, we note that nearly all our independent variables significantly explained variation in each energetics metric. Among these variables, we consistently see that frequency was the independent variable with the largest effect. We also find that the position of the dorsal and anal fins affected nearly all energetics metrics both directly and through an interaction with fin phasing. Interestingly, the direct effect of the far fin position was a reduction in propulsive economy and force oscillation. Inversely, SPS was increased as a direct result of greater fin spacing. The interaction effect suggests that, regardless of the independent effect, the far-fin position can lead to increased energetics values in most cases by mitigating the negative effect that increased fin phasing has in the near-fin foil. Although increased fin phasing causes a negative and concave down change in nearly all energetic measurements for near-fin foils, this effect becomes positive concave down in the far-fin foil for power consumption, ΔF_x, and ΔF_y. The effect of fin phasing on SPS remains negative in the far-fin foil, but the rate of decrease is much lower than in the near-fin foil. Together, these effects suggest that when the fins are largely synchronous the far-fin foil is less efficient but faster than the near-fin foils. However, when the fins are more out of phase, the far-fin foil will be both the more efficient and faster configuration. Finally, our model shows a counterintuitive trend that caudal fin peak-to-peak amplitude is negatively correlated with all energetic metrics. *P* values and error estimates for all models are given in table S4.

To aid in comparison we calculated maximum effects of variation in phase angle among each combination of fin positions and body stiffnesses (table 3). The flexible near-fin foil displayed fin phase values from 58°–90°, reaching a maximum SPS of 0.53 ms^{-1}. Our model predicted that this change of 32° led to a 26.2% decrease in SPS compared to the predicted value if the phase angle had not changed. Interestingly, the flexible far-foil model was predicted to have a very similar decreases in SPS attributed to changes in phasing, but over a much wider range of phase angles. Specifically, the model predicted that the measured maximum SPS of 0.59 ms^{-1} was 24.4% lower than it would have been if phasing was held at the low end of the 64° (51°–115°) phase range. Effects in the stiff body foils were more modest, with the near-fin foil's 40° (22°–62°) phase range causing a predicted

Table 3. Comparison between the highest measured SPS for each foil and the model predicted maximum SPS that would be achievable if the model had active control over fin-phasing and chose the optimal value from within the actual observed range. Predicted values are based on the model presented in tables 2 and S4.

Fin position	Stiffness	Phase range (difference)	Measured SPS (ms^{-1})	Predicted SPS at optimal phasing (ms^{-1})	% difference
Near-fin foil	Flexible	58°–90° (32°)	0.53	0.72	−26%
	Stiff	22°–62° (40°)	0.59	0.67	−12%
Far-fin foil	Flexible	51°–115° (64°)	0.59	0.78	−24%
	Stiff	46°–93° (47°)	0.65	0.75	−13%

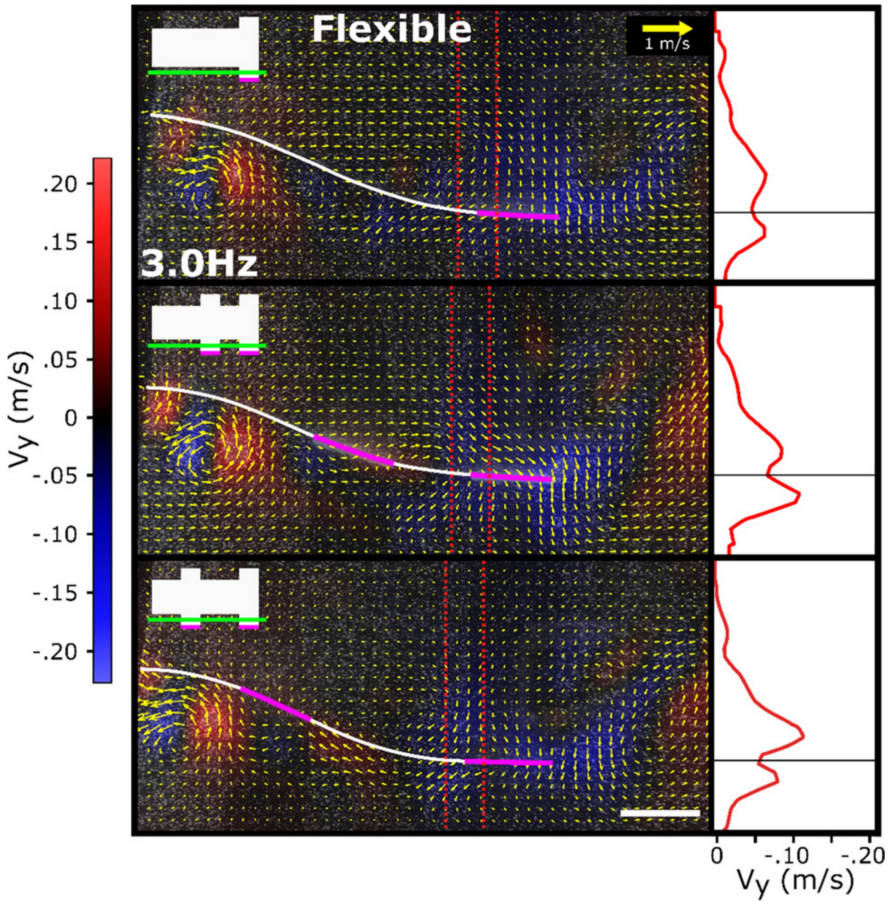

Figure 8. Flow visualization in flexible foils flapping at 3 Hz reveals a difference in the wake interacting with the caudal fin between foils with a dorsal/anal fin and the control foil without these fins. However, there was not an obvious difference between foils with different fin positions. Each image is taken in a plane that overlaps the anal and caudal fins (inset image, green line), captured at the moment that the leading edge of the caudal fin begins to move laterally. Yellow arrows indicate local water flow after subtracting the mean free stream velocity. Red and blue regions indicate the magnitude of lateral flow velocity (up and down in the images). Plots on the right show average lateral (sideways) velocity between the dashed red lines for each point on the vertical axis of the images. The horizontal black line on the plot shows where the leading edge of the caudal fin interacts with this flow. Each foil is highlighted with a white line and fin position is shown in magenta. Scale bar is 3 cm.

reduction in maximum potential SPS of 11.7% to the measured value of 0.59 ms^{-1}. Finally, the model estimated that the maximum SPS (0.65 ms^{-1}) in the stiff far-fin foil was 13.0% lower than it would have been if fin phasing remained at the bottom of the 47° range (46°–93°).

3.3. Flow visualization

Our energetics models showed that fin position interacted with fin phasing to change swimming performance. To understand the mechanisms behind this effect we used flow visualization with particle image velocimetry (PIV) to understand how fluid flow around the fins differs based on these parameters. When the caudal fin is first starting lateral motion there are differences among foils in the flow structure at the leading edge of the fins. In the flexible foil at 3.0 Hz the flow pattern was different between the control foil and the foils with fins. Specifically, when fins are present, there is stronger lateral (side-to-side) flow

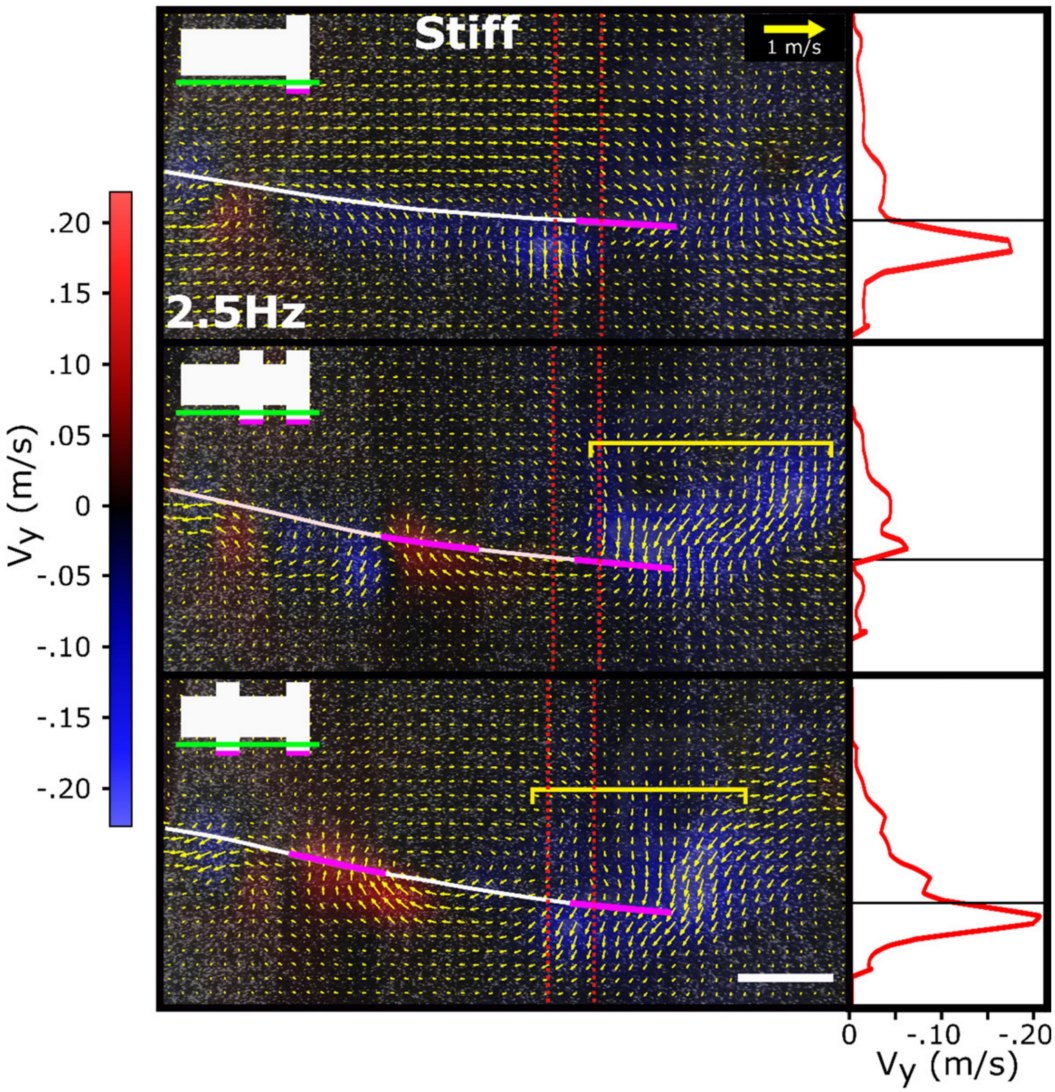

Figure 9. Flow visualization in stiff foils flapping at 2.5 Hz reveals a difference in wake interaction with the caudal fin in all foils. Notably, in foils with a dorsal/anal fin there is a large volume of water moving laterally (blue region highlighted with yellow bracket). The position of this wake structure is different between the two foils with different fin positions such that it only interacts with the caudal fin when the dorsal/anal fins are more anterior. Each image is taken in a plane that overlaps the anal and caudal fins (green line), captured at the moment that the leading edge of the caudal fin begins to move laterally. Yellow arrows indicate local water flow after subtracting mean free stream velocity. Red and blue regions indicate the lateral velocity of the flow (up and down in the images). Plots on the right side show average lateral velocity between the dashed red lines for each point on the vertical axis of the images. The horizontal black line on the plot shows where the leading edge of the caudal fin interacts with this flow. Each foil is highlighted with a white line and fin position is shown in magenta. Scale bar is 3 cm.

across the leading edge of the caudal fin due to flow shed from the dorsal and anal fins (figure 8). However, based on the recorded water velocities at this location there was not a substantial difference in the strength of this flow between different fin positions despite differences in fin phasing (near-fin = 90°, far-fin = 111°). In the stiff foil at 2.5 Hz there is a distinct lateral flow pattern that is only present in foils with a dorsal and anal fin (yellow bars, figure 9). Specifically, in the foil with more distantly spaced fins, the mass of laterally moving water appears to interact directly with the leading edge of the caudal fin as it begins its lateral motion. In the foil with near-fins this mass of water has already passed the leading edge of the caudal fin at the same time point (figure 9). These differences in flow may be related to the differences in fin phasing between the different foils (near-fin = 62°, far-fin = 79°).

Lateral flow along the leading edge of the caudal fin changes the effective angle of attack of the fin and can affect the formation of a thrust-producing LEV. In many fish, such as bluegill sunfish (figure 10), this vortex persists on the lateral surface of the caudal fin allowing it to produce thrust through much of the flapping cycle. We looked for this same flow pattern in our stiff foils flapping at 2.5 Hz. We found that

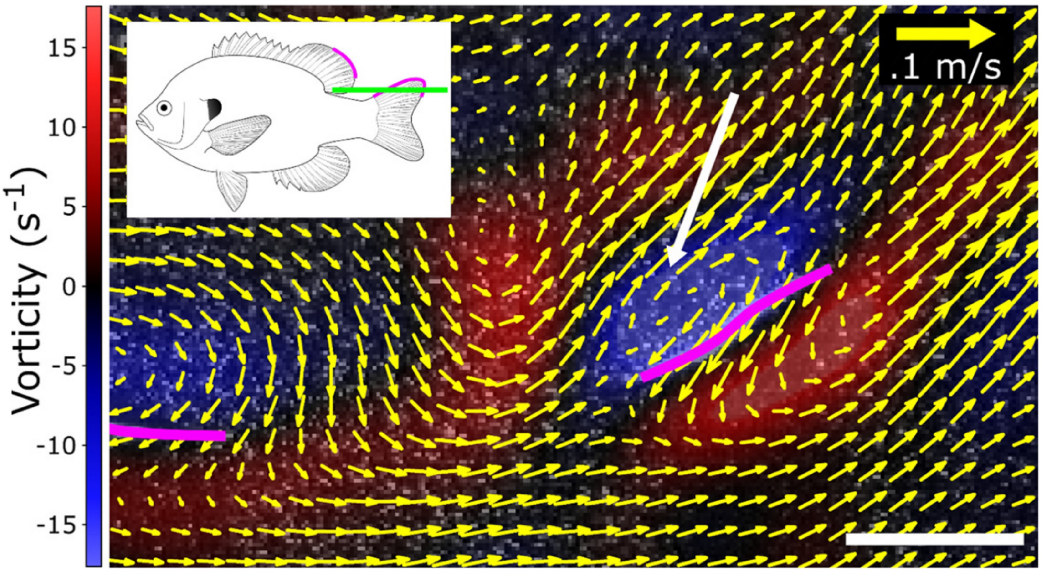

Figure 10. Lateral motion of the tail causes a thrust-producing leading edge vortex (white arrow) on the caudal fin of swimming fish, as in this bluegill sunfish (*Lepomis macrochirus*) swimming at 1.1 L s^{-1}. Flow is analyzed in a plane that overlaps the dorsal and caudal fins (green line). Yellow arrows indicate local water flow after subtracting mean free-stream velocity. Red and blue regions indicate vorticity of the flow (s^{-1}). Fins are highlighted in magenta. Scale bar is 1 cm.

without a dorsal or anal fin there is a weak LEV on the caudal fin when it is in the middle of a flapping cycle (figure 11). In the foil with close fins this LEV is absent, possibly due to negative flow interaction with the dorsal fin wake. In contrast, the LEV persists in the foil with the fins spaced further apart.

4. Discussion

Wake energy recapture has been an active topic of research for decades in both schooling fish and birds, as investigators have focused on understanding how flow leaving one individual impacts thrust and power consumption in following individuals [59–62]. More recently, researchers have emphasized the ability of animals to take advantage of a similar energy-saving effects using only the wake coming off their own body (table 1) [12, 13, 42]. None of these studies using model foil systems, however, have used a fish-like flexible body or have broadly characterized the performance effects of kinematic and morphological variation. Here we present a fish-like model that mimics biological morphology and generates thrust by undulating its body. We use a statistical model to draw conclusions about the effect of both controlled and emergent variables on swimming performance. We predicted that the wake from the dorsal and anal fins would alter thrust-producing flow structures on the caudal fin and that this effect would depend on the relative position and motion of the fins. We also predicted that the asynchronous production of forces by different fins would make force production of the whole system less variable through time and thus reduce center of mass oscillations (which increase energetic costs) (figure 1).

4.1. Critical variables controlling swimming performance

When building our statistical models of swimming energetics, we chose to include variables that we thought would be relevant to swimming performance, including both control parameters and fin kinematics. Our choices of which variables to include was largely verified by the AICc analysis (table S3). This statistical framework is designed to eliminate variables with little explanatory value and it excluded very few variables in our models. Although we might expect some collinearity in our explanatory variables, the lack of exclusions by AIC suggests that we were still able to extract independent effects of each variable. Among these variables, the position and phasing of the fins are the most relevant to fin–fin flow interactions as they combine to explain the relative motion of the dorsal and anal fin with the tail. Our models suggested that increasing fin distance and phase angle each independently decreased most energetics metrics, with the effect of phase angle generally being quadratic and concave down (table 2). However, this effect only applies to the near-fin configuration. When we consider the interaction of fin position and phase angle, we get an estimate of the relationship between phase angle and energetics for far-fin foils. This allows us to directly address our two predictions. The first prediction focused on fin–fin interactions and thrust production; therefore, we first examine the effect of fin phasing and fin position on SPS. Interestingly, we see that there is a significant and

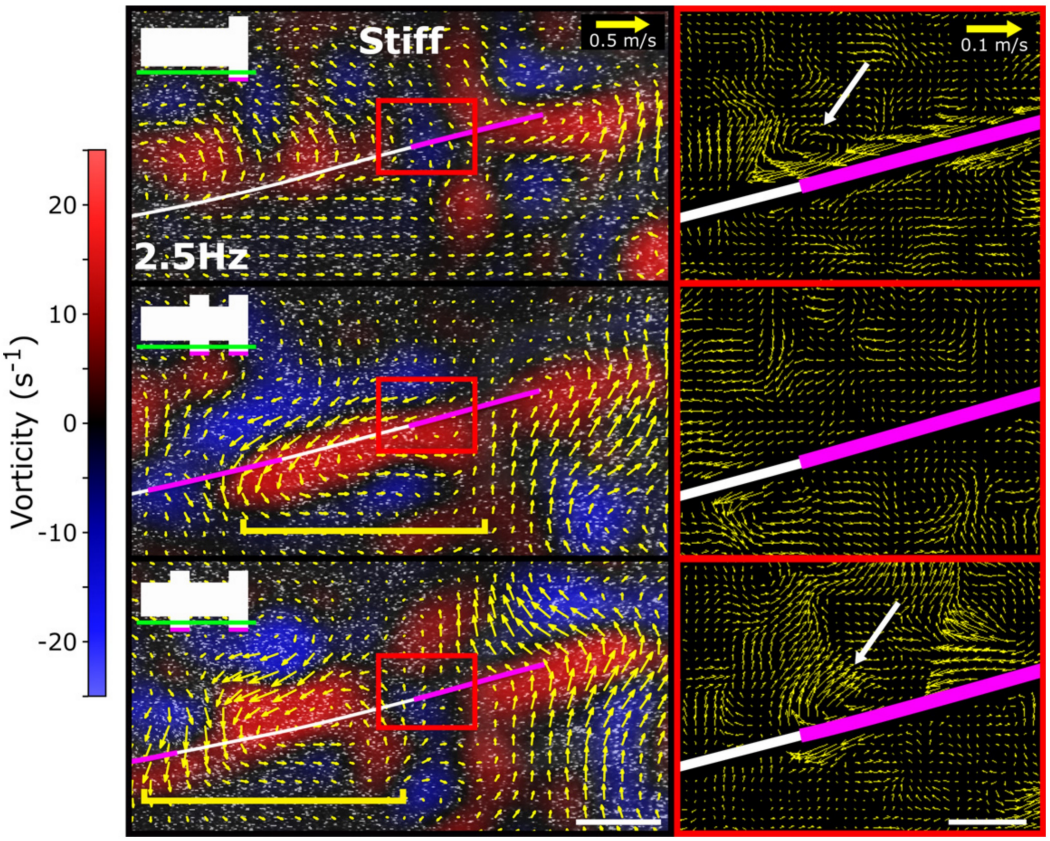

Figure 11. Flow visualization demonstrates that in stiff foils flapping at 2.5 Hz the presence and position of the dorsal and anal fins affects thrust-producing leading edge vortex formation on the caudal fin. In the control foil without a dorsal or anal fin there is relatively little flow in the anterior (left) portion of the frame. Visible in the inset on the right, is a small leading edge vortex on the caudal fin (white arrow). When dorsal and anal fins are positioned near the caudal fin there is relatively large region of vorticity around and directly anterior to the caudal fin (red region highlighted with yellow bracket). This comes from the wake off the dorsal and anal fins, and corresponds with the lack of a leading edge vortex in the inset. When the dorsal and anal fins are further from the caudal fin there is once again stronger vorticity from the dorsal and anal fin wakes (red region highlighted with yellow bracket), however the wake does not envelop the caudal fin. Without this flow interaction, there is once again a small leading edge vortex visible on the caudal fin in the inset (white arrow). Each image is taken in a plane that overlaps the anal and caudal fins (green line), captured as the caudal fin moves laterally. Yellow arrows indicate local water flow after subtracting mean free stream velocity. Red and blue regions indicate vorticity of the flow (s^{-1}). Fin position is highlighted in magenta. Scale bar is 2 cm in the panels to the left and 0.5 cm in the inset panels to the right.

positive interaction between these two predictor variables. The effect of this interaction is that, in addition to a positive direct effect on SPS of increasing fin distance, the far-fin foil experiences less of a reduction in SPS for the same change in phase angles (table 2). Therefore, the effect of phase angle on SPS is mediated by the position of the fins, with the far-fin configuration reaching maximum energetic values at a higher phase angle than the near-fin configuration. This is what would be expected if energetics were determined by the relative motion of the fins and is consistent with our prediction that fin phasing affects performance through fin–fin flow interactions. However, these data alone do not prove this mechanism.

In order to address our second prediction, we can similarly examine the effects of fin position, fin phasing, and their interaction in the models explaining ΔF_x and ΔF_y. Phase angle in the near-fin foil has a concave down effect on force oscillation with the highest force oscillation being found just below the mean fin phasing values (table 2). This means that at low phase angles the force oscillation is increasing, but as the fins become increasingly asynchronous the magnitude of the oscillations starts to decrease. The relationship between phasing and force oscillation in far-fin foils is similar, however the highest force oscillations are observed when the fins are far more asynchronous. This means that over the range observed in our study, increasing phase always leads to increasing force oscillation but in a concave down manner. Although the phase angle that led to maximum force oscillations was different based on the position of the fin, both foil shapes are expected to experience reduced force oscillations as they approach 180° phase lag (figure 1). Therefore, our second prediction is supported at high values of phasing. However, given the observed fin phasing values (figure 5), we would only expect this mechanism to reduce force oscillations in the near-fin foils, particularly the flexible one.

Next, we can compare the relative effects of each independent variable in all our energetics models and we find that flapping frequency had the largest effect on every energetics metric (table 2). This is expected because we held the leading-edge amplitude constant through all our experiments and therefore higher frequency movements translate to a more rapid flapping motion and higher force production. It is also consistent with studies of live fish which have shown that tail-beat frequency is one of the major behavioral modifications that fish use to change their swim speed [20, 54, 55]. Similarly, the fact that an increase in stiffness led to increases in force oscillation and power consumption was not surprising given that other studies using similar flapping foils have found that stiffer foils experience higher forces in general [47, 48, 50]. It was, however, surprising that despite the combination of increased force oscillation and power consumption without a predicted increase in swimming speed, stiffer foils were predicted to have a higher propulsive economy than flexible ones. Additionally, changing body stiffness allowed us to test the models with different ranges of body kinematics (figure 5). Surprisingly, increased caudal fin peak-to-peak amplitude led to a decrease in all energetics variables (table 2). Generally, we expect an increase in the forces generated by an undulatory swimmer when we increase the amplitude of flapping since thrust is correlated with caudal amplitude in fish swimming at low velocities [54, 58, 63–65]. If all else is equal, then an increase in force production from an undulatory body should correlate with increased thrust oscillations and increased power consumption. Our data do not directly address why this was not true in our model; however, we think that this may be in part because this model estimate assumes the frequency is unchanged. Since the lateral motion at the leading edge is the same in all trials, a decrease in caudal amplitude at the same frequency implies broad differences in body kinematics. If these differences led to faster changes of direction at the tail, then it would likely increase power consumption and force oscillation. Therefore, we think that this result is unlikely to hold true in actively actuated models.

4.2. Flow visualization

Flow visualization allowed us to move beyond the statistical model of SPS to understand why total thrust was affected by fin phasing and its interaction with fin spacing. Past studies have found that leading edge vortices (LEVs) are major contributors to thrust and are susceptible to augmentation from the external flow environment [12, 13]. Therefore, we focused flow visualization analysis on two time points during the flapping cycle that are critical to the formation and persistence of LEVs. We first looked at the caudal fin as it began lateral motion after reaching its furthest displacement from the midline in the flapping cycle. The LEV develops at this time and its strength depends on the angle of attack of the fin and the velocity of the fin relative to the surrounding water, both of which are susceptible to augmentation by external flow. We observed that the dorsal and anal fins each shed a wake that passes near the caudal fin at this time (figures 8 and 9). However, the strength of this flow pattern at the leading edge of the caudal fin, and therefore its expected effect on the LEV, varied greatly based on the position of the dorsal and anal fins. Specifically, in the stiff foils, when these fins were positioned closer to the caudal fin, the wake was further downstream at this time and failed to increase flow over the leading edge of the caudal fin. When these fins were more anterior, they left a wake that directly interacted with the leading edge of the caudal fin (figure 9).

We then examined flow around the caudal fin later in the flapping cycle to visualize the strength and persistence of the LEV. In the data collected from bluegill sunfish there was a thrust-generating LEV at this time point (figure 10) indicating that the LEV continued to generate thrust throughout the flapping cycle. In the stiff model that lacked a dorsal and anal fin we observed the caudal LEV mid cycle (figure 11). This indicates that the LEV can persist in the absence of an altered flow environment. In the model with these fins situated closer to the caudal fin we did not observe any LEV on the caudal fin at this time. Conversely, in the far-fin foil we saw a caudal LEV similar to the vortex seen in the absence of dorsal and anal fins. This suggests that this important thrust-generating LEV flow structure was extremely susceptible to the local flow regime, and that the wake from the dorsal and anal fins was enough to eliminate it altogether.

These patterns of flow augmentation are consistent with our statistical model of SPS and they help explain why fin position and phasing affected thrust. Our statistical model suggested that the swim speed, and therefore net thrust, was generally higher in the far-fin foil. This effect is exaggerated in cases where the fins are moving highly out of phase since the interaction effect predicts that thrust will decrease more quickly in the near-fin foil as fin phasing increases (table 2). This is consistent with the elimination of a thrust-generating LEV as seen in the flow visualization. Furthermore, we believe that the altered flow at the beginning of lateral tail motion (figure 9) may have completely prevented the formation of the LEV vortex in the near-fin foil, explaining why we failed to see an LEV at a later time point in this model (figure 11).

When the dorsal and anal fins are more anterior, their wake may increase flow speed over the leading edge of the fin and leads to a stronger persisting LEV later in the flapping cycle. Notably, Videler and Wardle [64] also found that certain flow interactions could eliminate caudal LEVs; however, they found that this effect was caused by an increased angle of attack leading to stall. It is important to note that these hydrodynamic hypotheses are based on flow patterns

seen at the highest tested flapping frequency. At low flapping frequencies the LEV may fail to form due to decreased lateral fin velocity, likely reducing any differences between foils with different fin positions. Furthermore, the exact nature of flow interactions are based on the combination of fin position, fin phasing, flapping frequency, and swim speed [66], so the energetically preferred fin position may be different given alternate body kinematics.

4.3. Comparison to previous engineering studies

Much of the past work on tandem flapping foil systems has been conducted primarily with engineering applications in mind. This has allowed us to understand the mechanisms by which flow interactions can augment performance and creates opportunity to apply the same theory to flow interactions among median fins on individual fish. Generally, these past studies have used two independently actuated rigid foils in tandem and compared the energetics of the rear foil to the energetics of a standalone foil. Since the foils move independently, greater variation in variables such as fin spacing, fin phasing, motion parameters, and the flow regime is possible. These studies have utilized both robotic experiments and CFD to analyze the fluid dynamics of their systems (table 1). The current study differs from past work in a number of ways, most notably because we used a single body that is actuated at the leading edge with passive flexibility. The body of the foils tested here has a tandem set of fins extending from it, creating a subsystem comparable to past studies. In this way, our study system connects our understanding of tandem foil systems with the whole-body mechanics of a fish while still maintaining the experimental tractability of a simple robotic system.

Another distinguishing feature that sets this experimental system apart from previous studies is that many of the relevant kinematic parameters are a result of the interaction of the body and the fluid instead of being independently controlled. As a result, we cannot examine energetic effects by altering a parameter for the upstream fin alone while controlling for everything else. Instead, we allow all parameters to covary during experiments as a consequence of the body's interactions with the fluid (as in a swimming fish) then use a statistical model to isolate the effect of each parameter. This approach allows us to make predictions about the individual effects of each independent variable thereby enabling predictions across a broader parameter space than we directly measured, though we must be careful about making predictions too far outside our tested parameter space.

With this in mind, we can use the parameter estimates from our model to predict the combined effect of fin position and phasing, parameters that can also vary in different species of fish. We will focus specifically on SPS estimates since this is directly related to the total thrust being generated and is therefore one of the most important response variables examined. We present these estimates separately for the stiff and flexible foils because body stiffness was found to affect the timing of the caudal fin relative to the dorsal and anal fins. In the flexible foil we found that the total effect of fin phasing was similar between the near-fin and far-fin foils when considered over the full phase ranges that were observed during experiments (table 2). Specifically, the maximum SPS was predicted to be 26.2% and 24.3% lower respectively than would have been expected if fin phasing remained unchanged from the lowest value. However, the range of phases seen in the far-fin foil was twice that of the near-fin foil's range. So although the total effects were similar, they were realized over drastically different kinematic ranges. We can similarly compare the effect of fin position on SPS in the stiff foils, where the model predicted 11.7% and 13.0% reductions in maximum SPS due to increases in phase angle for the near-fin and far-fin foils respectively. These values were achieved over a similar range of 40° and 47°. Together these results show that the effects of fin position and fin phasing are complicated and situationally dependent. Particularly in the flexible body, our model predicted that far-fin foils would have lower SPS when all else is equal but that they would respond less negatively to changes in phase angle.

Our predicted effects are lower than those reported in other studies, although effect sizes are not directly comparable because most previous studies measure thrust instead of the SPS (table 1). With this caveat, Akhtar *et al* [33] found that changing the phasing of the two separate foil-like fins from 48°–138° could decrease thrust by over 300%. Our results over a similar range of fin phasing indicate that in our fastest trials, the maximum effect of changing the fin phasing is ten times smaller, on the order of 30%. Despite this difference in magnitude, both our studies found that modulation of LEV strength was the most likely explanation for performance variation. This mechanism is also consistent with many prior studies on fin–fin interactions [9, 12, 13, 42, 67]. Additionally, several of these studies have found that this effect is simultaneously dependent on the inter-fin distance and on the fin phasing [9, 66, 67], similar to the interaction effect in the models presented here. This interaction is best described by Kinsey and Dumas [66] who derived a single metric that predicts the effect of flow interactions called the global phase difference. Although if fins are too far apart then the effect of flow interaction is reduced regardless of fin phasing [36], a trend that may explain why the interaction effect in our models caused fin phasing to have a smaller effect on swimming energetics (table 2). In general, we have found that similar fluidic effects are acting in our model as in many past studies of tandem flapping foils (table 1). However, we find a smaller effect size of changing fin morphology and kinematics. This

indicates that past studies examining hydrodynamic interactions of multiple fins can reasonably be applied to fish, but that effect sizes are likely much lower when accounting for the added mass of the body and the accompanying increase in drag. The rigid bodies of many past models (table 1) may also account for some of the differences in the magnitudes of our results.

When comparing the conditions of our experiments to those highlighted in table 1, we see that our experiments were generally run at a higher Reynold's number (Re) and with higher Strouhal number. Specifically, other studies were run at Re's between 400–30 000 while our study ranged from 27 000–106 000. However, since all these values are well within the von Kármán vortex street fluid regime [68], we do not expect the difference to substantially affect our results. Furthermore, fish generally swim between Re values of 10^3–10^6 [69], meaning that our study is more in line with Re values observed in fish than past engineering studies. Conversely, the studies highlighted in table 1 are more similar to fish in terms of the Strouhal number (St), with most fish exhibiting St from 0.2–0.5 [69]. Our study reached much higher values, implying that our model was less efficient that past studies and live fish. However, this is not surprising given that we were generating thrust with a passively flexing body. While our values of efficiency are likely lower than would be expected in other systems with lower St, we still believe that the effect of each kinematic variable on efficiency would be similar.

4.4. Comparing to data from live fish

One of the major features of this study is that the tested models are flexible and have both a body and fins designed to mimic the proportions and form of fish (figure 2). This suggests that the magnitude of the effects observed here should be closer to what would be expected in freely-swimming fishes. Though our estimates may actually be lower than the effects experienced by fish since our model moves passively and many of the thrust generating flow patterns that are affected by fin–fin interactions would be stronger with an actively flapping body and fins. Furthermore, fish are not constrained to the phase parameter space that we tested, with their fins generally moving more out of phase than the fins in these foils. Fish are also subject to a wide variety of selective pressures and can respond with many different behaviors, so we do not suggest that negative effects in our model translate directly to poor swimming performance in fish.

While increasing total thrust has many clear benefits, it is less obvious why a fish might want to decrease the magnitudes of oscillation amplitudes in both thrust and lateral forces. One possible reason for minimizing oscillations in thrust force is to stabilize the visual field. Nearly all vertebrates have reflexive coordination of eye and body movements to reduce oscillations in visual input to the retina [70]. Retinal stability reduces the use of saccades, a quick eye movement that reorients the visual field during which time there is little processing of visual information [71]. In fish, minimizing the unsteady portions of the swimming cycle and using saccades to reset the visual field only during high acceleration phases may improve perception of the surrounding environment [72, 73]. We suggest that fish may be able to limit the need for saccades and the accompanying visual impairment by decreasing thrust oscillations with fin–fin interactions thereby creating a steadier visual field. The benefits of decreased lateral force oscillations are more likely to be energetic in nature. Specifically, the amount of lateral motion during a flapping cycle will be directly controlled by the magnitude of the oscillations of lateral force. Increased lateral motion will increase the volume of entrained water around the body, and therefore increase the energetic cost of locomotion [67, 74]. Our results suggest that this cost can be reduced by changing relative fin motion (table 2).

As our models reveal, all the energetics metrics discussed above can be altered by changing fin and body kinematics. However, we do not suggest that this is only possible through evolutionary modification. Fishes have several behavioral capabilities that might allow them to avoid negative effects or enhance their swimming performance. For example, fish generally modulate their swim speed by changing tail beat frequency. Additionally, fishes have active control over median fin motion [7, 14–22] and could likely leverage this to optimize relative motion and timing of different fins. We found that increasing the distance between the dorsal and caudal fins had a complex effect on performance. Although fishes cannot move their fins longitudinally, many fish are capable of lowering both their first and second dorsal fins [16, 17] thus altering the exposed surface area. This would change the amount of space anterior to the caudal fin in which flow can develop and in certain circumstances could allow for fin–fin interactions that outweigh the effect of losing a propulsive surface. We also found that the phasing of the different fins could change swimming performance. Although the phasing of the fins in our model was completely determined by the undulatory wave passing down the body, fish are capable of independently flapping their dorsal and anal fins. The motion of these fins is still largely tied to the motion of the body since fin bases are attached to the body surface, but active fin-flapping may allow them to make small adjustments to fin phasing. Although we generally saw a negative effect of fin phasing on the energetics variables, we note that fish tend to move their fins more out of phase than our model (figure 5) and the expected effect of phasing is sinusoidal. Therefore, it is possible that fish may realize positive effects from the same variables that appeared to negatively affect energetics in our

model. The ability of fish to actively control fin morphology and kinematics to effect inter-fin flow interactions and thereby improve swimming performance is a particularly interesting area for future research.

Acknowledgments

This work was funded by the National Science Foundation Graduate Research Fellowship under Grant No. DGE1745303 to DM and by the Office of Naval Research MURI Grant N00014-15-1-2234 to GVL, monitored by Bob Brizzolara, and Office of Naval Research (Tom McKenna, Program Manager, ONR 341), Grant No. N000141410533. We thank Valentina Di Santo for providing trout and bass videos, members of the lauder lab for other fish swimming videos and feedback on the methodology, and both Zane Wolf and Robin Thandiackal for comments on the manuscript. We also thank two anonymous reviewers for their thoughtful comments that greatly improved the quality of the manuscript.

Data availability statement

The data that support the findings of this study are openly available at the following URL/DOI:https://doi.org/10.7910/DVN/CYTVE5.

ORCID iDs

David G Matthews https://orcid.org/0000-0002-5926-4348
George V Lauder https://orcid.org/0000-0003-0731-286X

References

[1] Lauder G V, Nauen J C and Drucker E G 2002 Experimental hydrodynamics and evolution: function of median fins in ray-finned fishes *Integr. Comp. Biol.* **42** 1009–17
[2] Dornburg A, Sidlauskas B, Santini F, Sorenson L, Near T J and Alfaro M E 2011 The influence of an innovative locomotor strategy on the phenotypic diversification of triggerfish (family: balistiidae) *Evolution* **65** 1912–26
[3] Price S A, Friedman S T and Wainwright P C 2015 How predation shaped fish: the impact of fin spines on body form evolution across teleosts *Proc. R. Soc.* B **282** 20151428
[4] Feilich K L 2016 Correlated evolution of body and fin morphology in the cichlid fishes *Evolution* **70** 2247–67
[5] Wainwright P C and Longo S J 2017 Functional innovations and the conquest of the oceans by acanthomorph fishes *Curr. Biol.* **27** R550–7
[6] Hodge J R, Alim C, Bertrand N G, Lee W, Price S A, Tran B and Wainwright P C 2018 Ecology shapes the evolutionary trade-off between predator avoidance and defence in coral reef butterflyfishes *Ecol. Lett.* **21** 1033–42
[7] Lauder G V 2000 Function of the caudal fin during locomotion in fishes: kinematics, flow visualization, and evolutionary patterns *Am. Zool.* **40** 101–22
[8] Plaut I 2000 Effect of fin size on swimming performance, swimming behavior, and routine activity of zebrafish (Danio rerio) *J. Exp. Biol.* **203** 813–20
[9] Zhu Q, Wolfgang M J, Yue D K P and Triantafyllou M S 2002 Three-dimensional flow structures and vorticity control in fish-like swimming *J. Fluid Mech.* **468** 1–28
[10] Tytell E D 2006 Median fin function in bluegill sunfish Lepomis macrochirus: streamwise vortex structure during steady swimming *J. Exp. Biol.* **209** 1516–34
[11] Tytell E D, Standen E M and Lauder G V 2008 Escaping flatland: three-dimensional kinematics and hydrodynamics of median fins in fishes *J. Exp. Biol.* **211** 187–95
[12] Liu G, Ren Y, Dong H, Akanyeti O, Liao J C and Lauder G V 2017 Computational analysis of vortex dynamics and performance enhancement due to body–fin and fin–fin interactions in fish-like locomotion *J. Fluid Mech.* **829** 65–88
[13] Han P, Lauder G V and Dong H 2020 Hydrodynamics of median-fin interactions in fish-like locomotion: effects of fin shape and movement *Phys. Fluids* **32** 011902
[14] Jayne B C, Lozada A F and Lauder G V 1996 Function of the dorsal fin in bluegill sunfish: motor patterns during four distinct locomotor behaviors *J. Morphol.* **228** 307–26
[15] Drucker E G and Lauder G V 2001 Locomotor function of the dorsal fin in teleost fishes: experimental analysis of wake forces in sunfish *J. Exp. Biol.* **204** 2943–58
[16] Lauder G V and Drucker E G 2004 Morphology and experimental hydrodynamics of fish fin control surfaces *IEEE J. Ocean. Eng.* **29** 556–71
[17] Drucker E G and Lauder G V 2005 Locomotor function of the dorsal fin in rainbow trout: kinematic patterns and hydrodynamic forces *J. Exp. Biol.* **208** 4479–94
[18] Standen E M and Lauder G V 2005 Dorsal and anal fin function in bluegill sunfish Lepomis macrochirus: three-dimensional kinematics during propulsion and maneuvering *J. Exp. Biol.* **208** 2753–63
[19] Standen E M and Lauder G V 2007 Hydrodynamic function of dorsal and anal fins in brook trout (Salvelinus fontinalis) *J. Exp. Biol.* **210** 325–39
[20] Maia A and Wilga C A 2013 Function of dorsal fins in bamboo shark during steady swimming *Zoology* **116** 224–31
[21] Maia A and Wilga C A 2016 Dorsal fin function in spiny dogfish during steady swimming *J. Zool.* **298** 139–49
[22] Maia A, Lauder G V and Wilga C D 2017 Hydrodynamic function of dorsal fins in spiny dogfish and bamboo sharks during steady swimming *J. Exp. Biol.* **220** 3967–75
[23] Frith H R and Blake R W 1991 Mechanics of the startle response in the northern pike, Esox lucius *Can. J. Zool.* **69** 2831–9
[24] Tytell E D and Lauder G V 2008 Hydrodynamics of the escape response in bluegill sunfish, Lepomis macrochirus *J. Exp. Biol.* **211** 3359–69
[25] Chadwell B A, Standen E M, Lauder G V and Ashley-Ross M A 2012 Median fin function during the escape response of bluegill sunfish (Lepomis macrochirus). I: fin-ray orientation and movement *J. Exp. Biol.* **215** 2869–80
[26] Chadwell B A, Standen E M, Lauder G V and Ashley-Ross M A 2012 Median fin function during the escape response of bluegill sunfish (Lepomis macrochirus). II: fin-ray curvature *J. Exp. Biol.* **215** 2881–90
[27] Borazjani I 2013 The functional role of caudal and anal/dorsal fins during the C-start of a bluegill sunfish *J. Exp. Biol.* **216** 1658–69
[28] Maia A and Wilga C D 2013 Anatomy and muscle activity of the dorsal fins in bamboo sharks and spiny dogfish during turning maneuvers *J. Morphol.* **274** 1288–98
[29] Webb P W 2005 *Stability and Maneuverability Fish Physiology* vol 23 (Amsterdam: Elsevier) pp 281–332
[30] Tritico H M and Cotel A J 2010 The effects of turbulent eddies on the stability and critical swimming speed of creek chub (Semotilus atromaculatus) *J. Exp. Biol.* **213** 2284–93

[31] Wolfgang M J, Anderson J M, Grosenbaugh M A, Yue D K and Triantafyllou M S 1999 Near-body flow dynamics in swimming fish *J. Exp. Biol.* **202** 2303–27
[32] Akhtar I and Mittal R 2005 A biologically inspired computational study of flow past tandem flapping foils *35th AIAA Fluid Dynamics Conf.*
[33] Akhtar I, Mittal R, Lauder G V and Drucker E 2007 Hydrodynamics of a biologically inspired tandem flapping foil configuration *Theor. Comput. Fluid Dyn.* **21** 155–70
[34] Rival D, Hass G and Tropea C 2011 The recovery of energy from leading- and trailing-edge vortices in tandem-airfoil configurations *J. Aircr.* **48** 203
[35] Broering T M, Lian Y and Henshaw W 2012 Numerical investigation of energy extraction in a tandem flapping wing configuration *AIAA J.* **50** 2295–307
[36] Boschitsch B M, Dewey P A and Smits A J 2014 Propulsive performance of unsteady tandem hydrofoils in an in-line configuration *Phys. Fluids* **26** 051901
[37] Shoele K and Zhu Q 2015 Performance of synchronized fins in biomimetic propulsion *Bioinspir. Biomim.* **10** 026008
[38] Muscutt L E, Weymouth G D and Ganapathisubramani B 2017 Performance augmentation mechanism of in-line tandem flapping foils *J. Fluid Mech.* **827** 484–505
[39] Kurt M and Moored K W 2018 Flow interactions of two- and three-dimensional networked bio-inspired control elements in an in-line arrangement *Bioinspir. Biomim.* **13** 045002
[40] Flammang B E, Alben S, Madden P G A and Lauder G V 2013 Functional morphology of the fin rays of teleost fishes *J. Morphol.* **274** 1044–59
[41] Gong W Q, Jia B B and Xi G 2016 Experimental study on instantaneous thrust and lift of two plunging wings in tandem *Exp. Fluids* **57** 8
[42] Zhong Q, Dong H and Quinn D B 2019 How dorsal fin sharpness affects swimming speed and economy *J. Fluid Mech.* **878** 370–85
[43] Wang J, Wainwright D K, Lindengren R E, Lauder G V and Dong H 2020 Tuna locomotion: a computational hydrodynamic analysis of finlet function *J. R. Soc. Interface* **17** 20190590
[44] Weihs D 1973 The mechanism of rapid starting of slender fish *Biorheology* **10** 343–50
[45] Webb P W and Weihs D 1983 Optimization of locomotion *Fish Biomechanics* ed P W Webb and D Weihs (New York: Praeger) pp 339–71
[46] Arreola V I and Westneat M W 1996 Mechanics of propulsion by multiple fins: kinematics of aquatic locomotion in the burrfish (Chilomycterus schoepfi) *Proc. R. Soc.* B **263** 1689–96
[47] Feilich K L and Lauder G V 2015 Passive mechanical models of fish caudal fins: effects of shape and stiffness on self-propulsion *Bioinsp. Biomim.* **10** 036002
[48] Lucas K N, Thornycroft P J M, Gemmell B J, Colin S P, Costello J H and Lauder G V 2015 Effects of non-uniform stiffness on the swimming performance of a passively-flexing, fish-like foil model *Bioinsp. Biomim.* **10** 056019
[49] Quinn D B, Lauder G V and Smits A J 2014 Flexible propulsors in ground effect *Bioinsp. Biomim.* **9** 036008
[50] Shelton R M, Thornycroft P J M and Lauder G V 2014 Undulatory locomotion of flexible foils as biomimetic models for understanding fish propulsion *J. Exp. Biol.* **217** 2110–20
[51] Quinn D B, Lauder G V and Smits A J 2015 Maximizing the efficiency of a flexible propulsor using experimental optimization *J. Fluid Mech.* **767** 430–48
[52] Wen L and Lauder G 2013 Understanding undulatory locomotion in fishes using an inertia-compensated flapping foil robotic device *Bioinsp. Biomim.* **8** 046013
[53] Lauder G V, Anderson E J, Tangorra J and Madden P G A 2007 Fish biorobotics: kinematics and hydrodynamics of self-propulsion *J. Exp. Biol.* **210** 2767–80
[54] Bainbridge R 1963 Caudal fin and body movement in the propulsion of some fish *J. Exp. Biol.* **40** 23–56
[55] Akanyeti O, Putney J, Yanagitsuru Y R, Lauder G V, Stewart W J and Liao J C 2017 Accelerating fishes increase propulsive efficiency by modulating vortex ring geometry *Proc. Natl Acad. Sci. USA* **114** 13828–33
[56] Read Q D, Baiser B, Grady J M, Zarnetske P L, Record S and Belmaker J 2018 Tropical bird species have less variable body sizes *Biol. Lett.* **14** 20170453
[57] Burnham K P and Anderson D R 2010 *Model Selection and Multimodel Inference: A Practical Information-Theoretic Approach* (New York: Springer)
[58] Webb P W, Kostecki P T and Stevens E D 1984 The effect of size and swimming speed on locomotor kinematics of rainbow trout *J. Exp. Biol.* **109** 77–95
[59] Keenleyside M H A 1955 Some aspects of the schooling behavior of fish *Behavior* **8** 183–247
[60] Cushing D H and Jones F R H 1968 Why do fish school? *Nature* **218** 918–20
[61] Fish F E 1995 Kinematics of ducklings swimming in formation: consequences of position *J. Exp. Zool.* **273** 1–11
[62] Becker A D, Masoud H, Newbolt J W, Shelley M and Ristroph L 2015 Hydrodynamic schooling of flapping swimmers *Nat. Commun.* **6** 8514
[63] Webb P W 1986 Kinematics of lake sturgeon, Acipenser fulvescens, at cruising speeds *Can. J. Zool.* **64** 2137–41
[64] Videler J J and Wardle C S 1991 Fish swimming stride by stride: speed limits and endurance *Rev. Fish Biol. Fish.* **1** 23–40
[65] Bainbridge R 1958 The speed of swimming of fish as related to size and to the frequency and amplitude of the tail beat *J. Exp. Biol.* **35** 109–33
[66] Kinsey T and Dumas G 2012 Optimal tandem configuration for oscillating-foils hydrokinetic turbine *J. Fluids Eng.* **134** 031103
[67] Mignano A, Kadapa S, Tangorra J and Lauder G 2019 Passing the wake: using multiple fins to shape forces for swimming *Biomimetics* **4** 23
[68] Vogel S 1994 *Life in Moving Fluids: The Physical Biology of Flow* (Princeton, NJ: Princeton University Press)
[69] Eloy C 2012 Optimal Strouhal number for swimming animals *J. Fluid Struct.* **30** 205–18
[70] Masseck O A and Hoffmann K-P 2009 Comparative neurobiology of the optokinetic reflex *Ann. New York Acad. Sci.* **1164** 430–9
[71] Ebenholtz S M 2009 *Oculomotor Systems and Perception* (Cambridge: Cambridge University Press)
[72] Mandecki J L and Domenici P 2015 Eye movements are coordinated with pectoral fin beats during locomotion in a marine teleost fish *J. Exp. Biol.* **218** 1122–5
[73] Sun S, Zuo Z, Ma M M, Qian C, Chen L, Zhou W, Drasbek K R and Zuxiang L 2019 Neural circuits mediating visual stabilization during active motion in zebrafish *bioRxiv* Preprint https://doi.org/10.1101/566760
[74] Xiong G and Lauder G V 2014 Center of mass motion in swimming fish: effects of speed and locomotor mode during undulatory propulsion *Zoology* **117** 269–81